ROYAL SOCIETY
OF CHEMISTRY

Check for updates

Systematic investigation on unsymmetrical mesogenic cyanobiphenyl dimers towards optical storage devices: synthesis, mesomorphic, photo switching and DFT studies†

Mahima Rabari,[a] Vasundhara Hegde,[b] Gurumurthy Hegde [ID]*[bc] and
A. K. Prajapati [ID]*[a]

This research presents the synthesis and analysis of a novel series of mesogenic dimers comprising cyanobiphenyl and azonaphthyl units. Structural validation was performed using FT-IR, ^{1}H-NMR, ^{13}C-NMR, elemental analysis, mass spectrometry, *etc.* The dimers' thermotropic behaviours were studied through POM and DSC, revealing enantiotropic nematic phases in all cases, with some also showing monotropic smectic C phases. The study explores the relationship between the chemical structure of the dimers and the length of the flexible spacer, the odd−even effect, and their phase transition temperatures. Longer chains tended to form smectic phases, while shorter chains primarily exhibited nematic phases. Computational analysis using B3LYP/6-31g(d,p) and evaluations of electrostatic potential (ESP) and optical properties provided further insight into the electronic structures. Photoisomerization studies demonstrated consistent photochromic responses, with all dimers showing high conversion efficiency (88−95%) under UV light along with similar back relaxation times (∼10−12 hours). Optical storage devices prepared by these materials showed excellent contrast between dark and bright states elucidating the importance of such materials for the future.

1. Introduction

The cyanobiphenyl moiety is significant in the formation of liquid crystalline (LC) materials due to their unique molecular structure, which promotes the formation of stable liquid crystal phases. The rigid, rod-like shape of the biphenyl core, combined with the strong dipolar interaction introduced by the cyano group (–CN), enhances molecular alignment and order, which is crucial for the development of nematic and smectic phases. The cyano group, being highly polar, also contributes to the thermal stability and dielectric properties of the liquid crystalline phase, making cyanobiphenyl derivatives highly valuable in the design of liquid crystal displays (LCDs) and other advanced optical devices. Commercially available liquid crystals such as 5-cyanobiphenyls (5-CB), owing to their dimeric structure, exhibit the desired nematic (N) phase even at room

temperature.[1] In particular, the utilization of the nematic (N) and twist-bend nematic (N_{TB}) phases in liquid crystal (LC) dimers and other systems has found practical applications, including the selective reflection of light controlled by electric and magnetic fields, along with advancements in the development of tuneable lasers.[2] Over the past decade, significant attention has been directed towards studying the N_{TB} phase, which is generally obtained in dimers containing a cyanobiphenyl moiety. Initially proposed in theoretical research,[3–5] the N_{TB} phase was later confirmed experimentally in bent LC dimers.[6] This phase is characterized by a helical precession of the director with a typical pitch of several tens of nanometres, which increases with temperature.[7–9]

Interestingly, the helical structures observed in the N_{TB} phase share optical and physical properties resembling the layered smectic phase rather than the typical nematic phase, thus categorizing the N_{TB} phase as a pseudo-layered phase.[10–13] However, less attention has been paid to variations in spacer length and the chemical composition of links between the spacer and mesogenic units.[14–19] Recent studies have documented the emergence of the twist-bend nematic phase in odd LC dimers containing ether linkages to their mesogenic units.[20,21] Additionally, several bent LC dimers have been identified to exhibit Iso-N_{TB} phase transitions in their single-

[a] *Department of Chemistry, Faculty of Science, The Maharaja Sayajirao University of Baroda, Vadodara-390002, India. E-mail: akprajapati@yahoo.co.uk*

[b] *Department of Chemistry, Christ University, Hosur Road, Bengaluru 560029, India. E-mail: murthyhegde@gmail.com*

[c] *Centre for Advanced Research and Development, Christ University, Hosur Road, Bengaluru 560029, India*

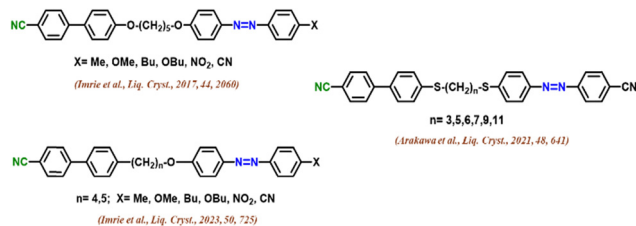† Electronic supplementary information (ESI) available. See DOI: **https://doi.org/10.1039/d5tc00421g**

This journal is © The Royal Society of Chemistry 2025

Fig. 1 Asymmetric dimers featuring a combination of cyanobiphenyl and azo moiety.

component systems. Examples include homologues of imine-linked dimers with a propane spacer and terminal methoxy/ethoxy groups,[22] propane- and ethylthio-linked cyanobiphenyl-based dimers,[23] and a bent phosphine-bridged cyanobiphenyl dimer.[24] Liquid crystal dimers incorporating cyanobiphenyl and azo groups represent a promising class of materials. These dimers typically feature two distinct segments: a cyanobiphenyl moiety, which provides a rigid core and imparts nematic behaviour, and an azo group, which introduces additional functionality and influences the mesomorphic properties. Arakawa *et al.* reported asymmetric cyanobiphenyl and naphthalene dimers that exhibit the twist-bend nematic phase.[25] They have also reported thioether-linked azobenzene-based liquid crystal dimers exhibiting the twist-bend nematic phase over a wide temperature range.[26]

Fig. 1 depicts a few examples of unsymmetrical cyanobiphenyl dimers with a cyanobiphenyl and azo moiety. Arakawa *et al.* introduced a non-symmetric series with sulphur linkages based on 4-cyanoazobenzene and 4-cyanobiphenyl arms, showing supercooled NTB phases.[26] Imrie *et al.* presented two sets of novel non-symmetric LC dimers. These dimers exhibited NTB and N phases, with varying terminal substituents.[27,28] They also introduced a non-symmetric series with sulphur linkages based on 4-cyanoazobenzene and 4-cyanobiphenyl arms, showing super-cooled NTB phases.[27,28] Introducing light on photochromic molecules is always an exciting area of research, especially when it comes to optical storage applications.[29–32] Azobenzene is one such light-sensitive moiety which can alter easily with the illumination of UV light of 365 nm wavelength. Due to this, the energetically stable *trans*-molecule will convert to *cis*-molecules that are not stable as such. Due to this, *cis* molecules can be brought back to the original configuration either by shining a white light of wavelength 450 nm or by keeping the system as it is in the dark. The later process is known as thermal back relaxation and is extremely important for the creation of optical storage devices.[33–35] Unsymmetrical dimers play a very peculiar role here since they have a competing effect between Azo and the main chain. The addition of the spacer length in these systems was not studied fully as far as our knowledge is concerned and this study is a perfect platform to understand the structure–property relationship between them.

Naphthalene moiety and azo linkage play critical roles in the formation of liquid crystalline compounds due to their structural and electronic characteristics. The naphthalene ring, with its extended conjugated system, introduces rigidity and planarity to the molecule, which is essential for maintaining the anisotropic

properties needed for liquid crystal phases.[36–38] The novelty of this work lies in the incorporation of a naphthalene moiety at one terminal of the LC dimer, introducing asymmetry to the molecular design. While cyanobiphenyl-based dimers with azo linkages are well-studied, the use of an unsubstituted naphthalene unit remains scarce. Its larger π-system increases molecular breadth, potentially disrupting intermolecular interactions, yet the synthesized dimers exhibit stable mesomorphic properties. This synergy between cyanobiphenyl and naphthalene offers valuable insights into the structure–property relationships of LC dimers, demonstrating a fine balance between rigidity and flexibility to maintain liquid crystallinity.

To deepen our understanding of the relationships between structure and properties in dimers based on cyanobiphenyl and incorporating naphthalene entities, and to evaluate how different flexible spacers influence their phase behaviour, here we synthesized a new series of calamitic–calamitic dimers. These dimers contain cyanobiphenyl ether and azo naphthyl. The mesogenic units in these compounds are linked *via* ether bonds and are separated by a flexible spacer ranging from 2–6, and 8–12 methylene groups in length. The abbreviated name CBOH represents compounds where "CB" denotes the cyanobiphenyl group. In, NpAzOH, the word "NpAz" indicates the rod-like azonaphthyl. Series **CBnAZ** dimers are dimers in which one end bears a cyanobiphenyl group and the other end bears an azonaphthyl moiety and "*n*" signifies the no. of carbon atoms/length of the flexible spacer for these unsymmetrical dimers.
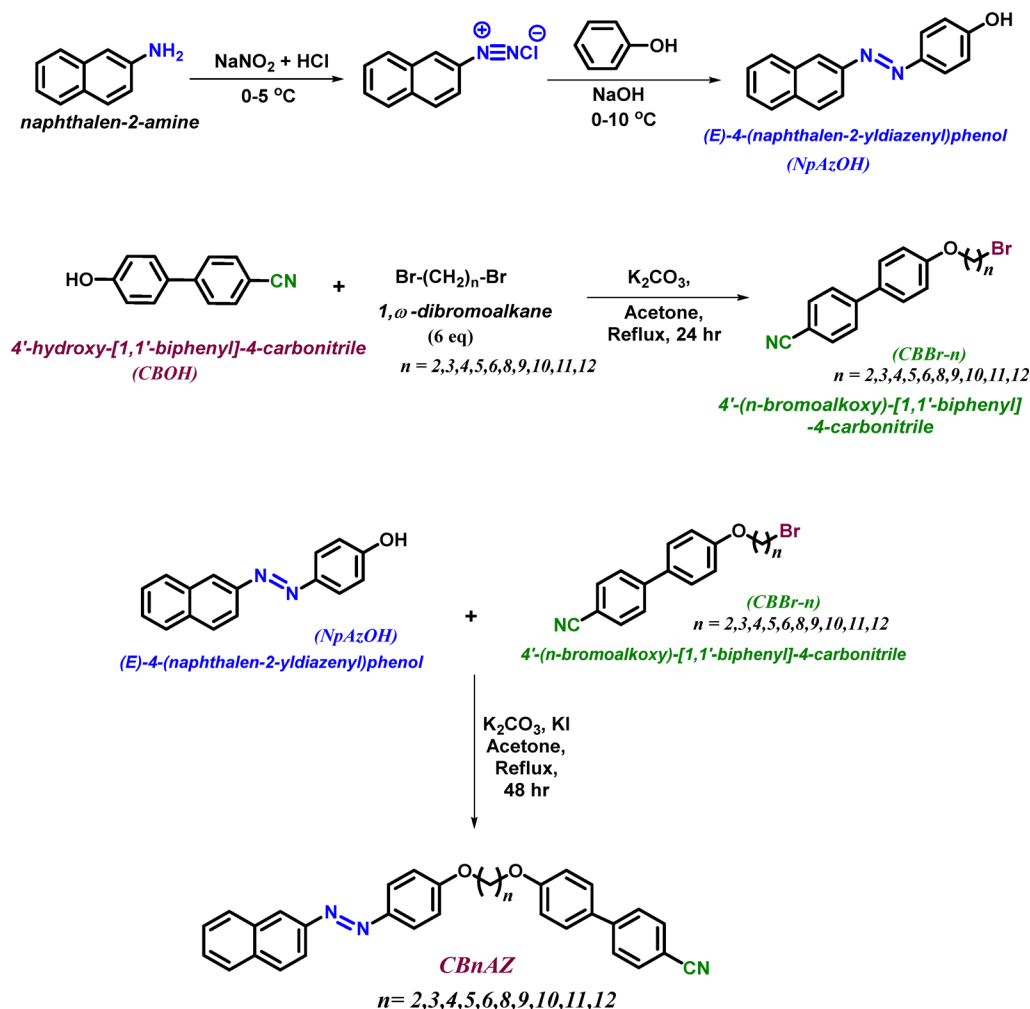
2. Synthesis

The liquid crystalline dimers of the **CBnAZ** series were synthesized using a standardized procedure described in Scheme 1. Synthesis of key intermediate (*E*)-4-(naphthalen-2-yldiazenyl)-phenol (NpAzOH) has been done according to the literature.[38] **CBBr-n** was synthesized by refluxing a mixture containing 4′-hydroxy-[1,1′-biphenyl]-4-carbonitrile (CBOH), α,ω-dibromo-alkanes and K_2CO_3, in solvent acetone for a time period of 24 h, followed by filtration and purification using column chromato-graphy. In **CBBr-n**, *n* is the no. of carbons present in the flexible spacer. The reaction of **CBBr-n** with NpAzOH, carried out *via* the Williamson ether synthesis in the presence of anhydrous K_2CO_3 and KI in acetone, resulted in the formation of **CBnAZ** (*n* = 2–6, 8–12).

3. Results and discussion

3.1. Chemistry

The accurate structures were confirmed using a range of analytical techniques, such as FT-IR, ^{1}H NMR, ^{13}C NMR, mass spectrometry and elemental analysis. The molecular structure of **CB6AZ** serves as a representative example for the entire series. The FT-IR spectrum of the dimer **CB6AZ** exhibits C–H stretching bands for both the alkyl and benzylic groups in the range of 2800–3080 cm^{-1}. Absorption bands with medium intensity observed in the range of 1610–1595 cm^{-1} are likely

This journal is © The Royal Society of Chemistry 2025

J. Mater. Chem. C, 2025, **13**, 10700–10713 | **10701**

Scheme 1 Synthesis scheme for the dimers of series **CB*n*AZ**.

due to the stretching vibrations of the azo (–N═N–) group. Additionally, the stretching vibrations of the aromatic (–C═C–) bonds are detected within the frequency range of 1550–1500 cm^{-1}. The medium intensity band for the nitrile group (–C≡N) appeared around 2220–2228 cm^{-1}. The ^{1}H NMR spectrum of **CB6AZ** revealed triplet peaks within the chemical shift range of δ 4.35–3.95 ppm, attributable to the protons on the carbon bonded to an oxygen atom. The remaining methylene protons exhibited a multiple signal in the range of δ 2.50–1.25 ppm. The aromatic protons were observed in the region of δ 6.80–8.50 ppm. In the ^{13}C NMR of **CB6AZ**, peaks for methylene protons of the flexible spacer were observed around δ 25 to 30 ppm. The carbon, which is directly attached to the oxygen signal, was found around δ 65–69 ppm. The aromatic carbon signals were observed in the range of δ 110–165 ppm. The characteristic peak for the nitrile carbon (–C≡N) appeared around δ 117–119 ppm.

3.2.   Mesomorphic behaviour

The phase behaviour and mesomorphic properties of the dimers were analyzed using a differential scanning calorimeter (DSC) and a polarizing optical microscope (POM). The DSC measurements were conducted at a rate of 10 °C per minute during both the

heating and cooling cycles, and the thermograms were acquired using the DSC-822 system (make: Mettler Toledo) along with Stare software. The transition temperatures (in °C) and corresponding transition enthalpy values (ΔH in kJ mol^{-1}) for the **CB*n*AZ** dimers are summarized in Table 1. The DSC thermogram for the **CB6AZ** dimers can be seen in Fig. 2. During heating, the compound undergoes an endothermic transition from the Cr to N phase at 178.04 °C, accompanied by an enthalpy change (ΔH) of 51.57 kJ mol^{-1}. The subsequent phase change from the nematic to the isotropic liquid state occurs at 225.60 °C with a smaller ΔH of 2.48 kJ mol^{-1}. During the cooling process, the reverse transitions take place, demonstrating the reversibility of the phase changes. These transitions include Iso-to-N at 222.11 °C, N-to-SmC at 163.38 °C, and SmC-to-Cr at 147.52 °C, with all of them being exothermic, as shown in Fig. 2. It can be concluded that the compound exhibits an enantiotropic nematic phase along with a monotropic smectic C phase.
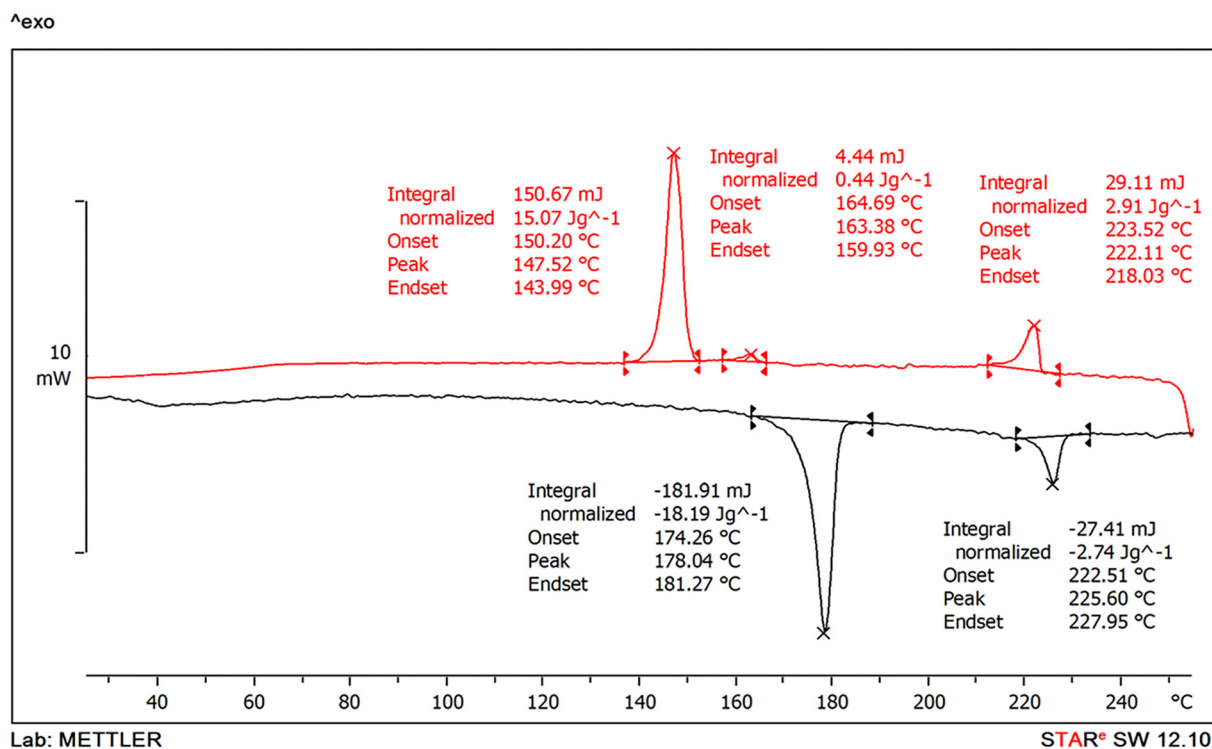
To determine the LC behaviour of the dimers being studied, the compounds were placed between coverslips and examined using POM. The samples were heated until they reached the isotropic phase and then slowly cooled at a rate of 10 °C per minute to observe the transition from the isotropic to the liquid

Table 1 The transition temperatures (°C) and the associated enthalpy values (ΔH) for **CBnAZ**

Dimer	n	Transition temperatures (in °C) [ΔH (in kJ mol^{-1})]	
		Heating cycle	Cooling cycle
CB2AZ	2	Cr 250.64 (55.22) N 268.70 (2.57) Iso	Iso 265.38 (−2.52) N 197.05 (−50.99) Cr
CB3AZ	3	Cr 196.98 (39.33) Iso	Iso 168.32 (−0.80) N 150.30 (−36.39) Cr
CB4AZ	4	Cr 208.06 (58.65) N 248.74 (2.91) Iso	Iso 245.97 (−2.70) N 173.14 (−56.58) Cr
CB5AZ	5	Cr 182.76 (45.50) Iso	Iso 170.58 (−1.30) N 132.38 (−37.60) Cr
CB6AZ	6	Cr 178.04 (51.57) N 225.60 (2.48) Iso	Iso 222.11 (−2.21) N 163.38 (−0.44) SmC 147.52 (−49.93) Cr
CB8AZ	8	Cr 162.88 (53.62) N 198.65 (2.98) Iso	Iso 195.65 (−2.96) N 155.87 (−0.94) SmC 138.13 (−55.09) Cr
CB9AZ	9	Cr 146.76 (46.58) N 173.28 (1.69) Iso	Iso 169.93 (−1.40) N 114.73 (−46.19) Cr
CB10AZ	10	Cr 157.40 (45.80) N 194.54 (2.43) Iso	Iso 192.63 (−2.42) N 148.14 (−0.24) SmC 118.33 (−43.27) Cr
CB11AZ	11	Cr 143.93 (42.72) N 169.64 (2.39) Iso	Iso 166.06 (−2.64) N 124.60 (−0.37) SmC 113.08 (−46.08) Cr
CB12AZ	12	Cr 150.58 (41.53) N 185.50 (2.16) Iso	Iso 183.79 (−2.05) N 144.31 (−0.22) SmC 120.64 (42.69) Cr

Cr: crystalline state; SmC: smectic C phase; N: nematic phase; Iso: isotropic Liquid

Fig. 2 DSC thermogram of **CB6AZ**.

crystalline phase. Fig. 3 depicts an optical microphotograph of the dimer **CB6AZ** during the first heating and cooling cycle. At 178 °C during heating (Fig. 3a), a change in the phase is observed, indicating a transition from a Cr to N phase. Subsequently, at 181 °C (Fig. 3b), a Schlieren texture emerges, followed by N to Iso phase transition at 225 °C (Fig. 3c), marking a shift from a nematic phase to an isotropic phase. Upon cooling, at 222 °C (Fig. 3d), nematic droplets form, indicating the presence of an enantiotropic nematic phase, which coalesces to give a Schlieren texture at 218 °C (Fig. 3e). Notably, at 164 °C (Fig. 3f), a transition from the N to SmC phase occurs, accompanied by a focal conic texture at 162 °C (Fig. 3g), characteristic of the SmC phase. Further cooling leads

to the SmC-to-Cr transition at 148 °C (Fig. 3h), transitioning to a crystalline state observed at 143 °C (Fig. 3i).

3.3. Structure–property relationship

A line graph can be an effective way to visually depict the trends in the properties of LC dimers, showing how factors like the length of the spacer chain and odd–even effects impact clearing temperatures and phase behaviour. The graph in Fig. 4a displays the relationship between the number of carbons in the flexible spacer chain (n) on the x-axis and the transition temperatures (°C) on the y-axis. Each data point corresponds to a particular dimer, showing its clearing temperature in relation to the length of the spacer chain. In Fig. 4b, the bar graph illustrates the mesophase stability

This journal is © The Royal Society of Chemistry 2025

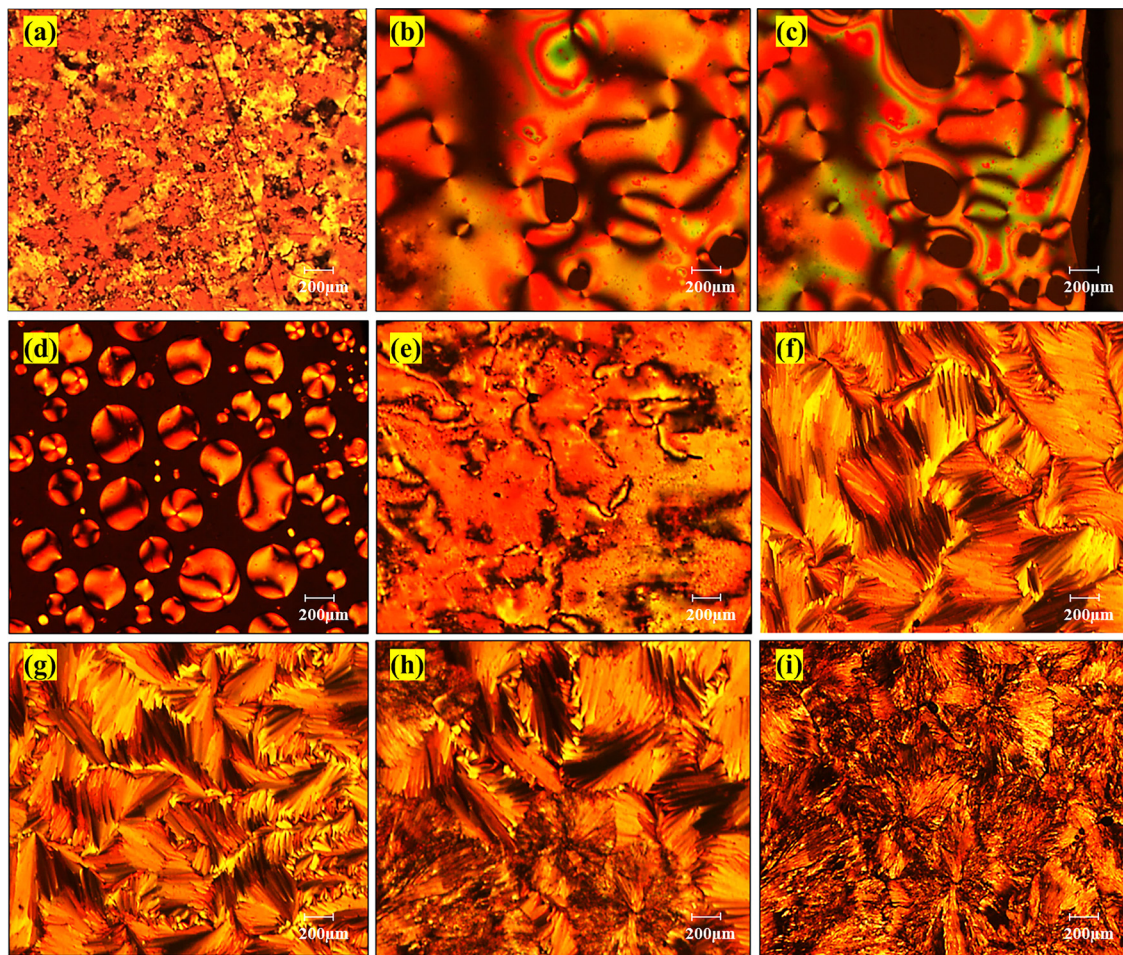J. Mater. Chem. C, 2025, **13**, 10700–10713 | **10703**

Fig. 3 Optical microphotographs of dimer **CB6AZ**: (a) nematic phase at 178 °C on heating, (b) at 181 °C, a Schlieren texture appears, (c) nematic to isotropic transition at 225 °C, (d) formation of nematic droplets at 222 °C upon cooling, (e) reappearance of Schlieren texture at 218 °C, (f) transition to SmC phase at 164 °C, (g) broken focal conic texture of the SmC phase at 162 °C, (h) transition from SmC to Cr at 148 °C, and (i) crystalline state at 143 °C.

for dimers **CBnAZ**. Mesophase stability refers to the propensity of a liquid crystal material to maintain its ordered mesophase, such as the nematic or smectic phase, over a range of temperatures during both the heating and cooling cycle.
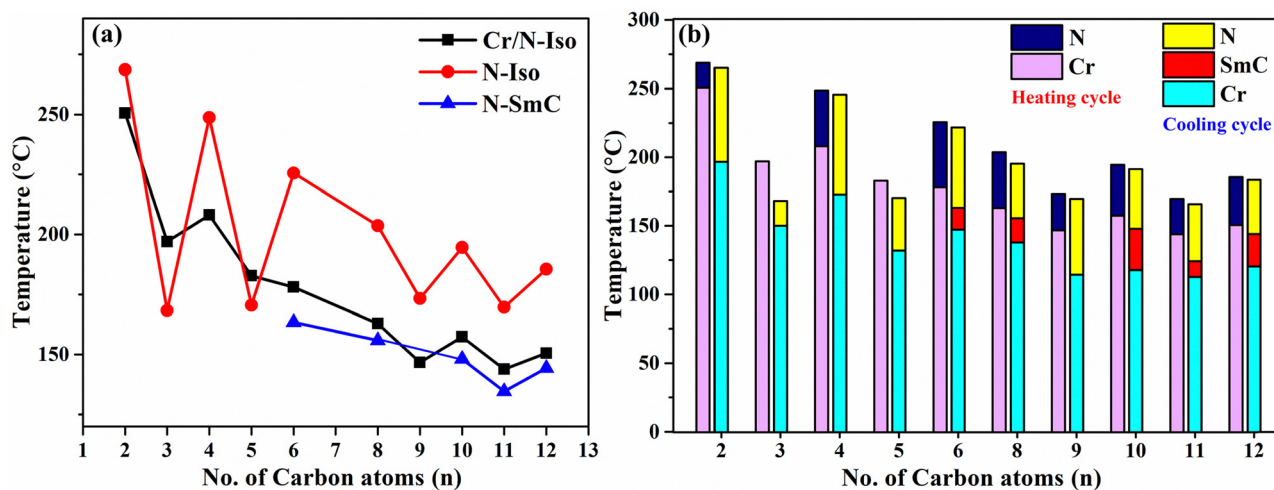

Fig. 4 (a) Line graph displaying the transition temperatures as a function of the number of carbons in the flexible spacer, and (b) bar graph highlighting the mesophase stability of the series **CBnAZ** dimer.

10704 | J. Mater. Chem. C, 2025, **13**, 10700–10713

This journal is © The Royal Society of Chemistry 2025

Firstly, when the flexible spacer lengthens, the clearing temperatures and melting points typically decrease. This is attributed to the increased flexibility of the spacer, which weakens the intermolecular forces between the molecules. As a result, the molecules are less likely to align and exhibit ordered phases at higher temperatures, leading to lower clearing temperatures.

Secondly, odd-membered dimers often exhibit comparatively lower clearing temperatures, a characteristic known as the odd–even effect. This effect arises due to the differing molecular arrangements and intermolecular interactions between odd and even members. Odd-membered dimers often do not exhibit the SmC phase. The odd-numbered spacer introduces a conformational bend in the molecular structure, disrupting the uniform tilt required for SmC formation. This structural distortion results in the stabilization of nematic (N) phases instead, as seen in our study where n = 3, 5, and 9 show only nematic phases. As the spacer length increases, the odd–even effect weakens because the flexibility of the longer alkyl chain allows for structural relaxation. For example, n = 11 exhibits both an enantiotropic nematic and a monotropic smectic phase, indicating that as the chain length increases, the odd–even influence diminishes, and smectic phases can start appearing in odd-membered dimers as well.

Lastly, an increase in chain length often leads to the emergence of smectogenic behaviour. Higher-membered dimers, typically ranging from n = 6 to n = 12, exhibit smectic phases in the cooling cycle, indicative of layered structures with long-range positional order. In contrast, lower-membered dimers, ranging from n = 2 to n = 5, predominantly display the nematic phase, as their shorter chains limit the development of layered smectic structures. This trend underscores the pivotal role of molecular structure, particularly chain length, in dictating the phase behaviour of liquid crystal dimers, with longer chains favouring smectic phases and shorter chains favouring nematic phases.

3.4. Thermogravimetric analysis (TGA)

The TGA curve (Fig. 5) shows that the decomposition of **CB6AZ** begins around 400 °C, with a significant weight loss of 82.00% observed between 400–450 °C, indicating its primary thermal decomposition. The DTG curve further highlights this decomposition, with a peak at 450.2 °C indicating the maximum rate of weight loss. After 450.2 °C, the weight stabilizes, leaving a residue of 4.42%, which suggests the presence of stable, non-volatile residues. The DTA curve also shows an endothermic peak at 172.6 °C, possibly related to a phase transition, further characterizing the thermal behaviour of **CB6AZ**. This analysis provides valuable insights into the compound's thermal properties and decomposition processes.

3.5. Computational studies

In our study, density functional theory (DFT) calculations were carried out using the B3LYP hybrid functional, which incorporates Becke's three-parameter approach, along with the 6-31G basis set. The computational framework employed Gaussian 09
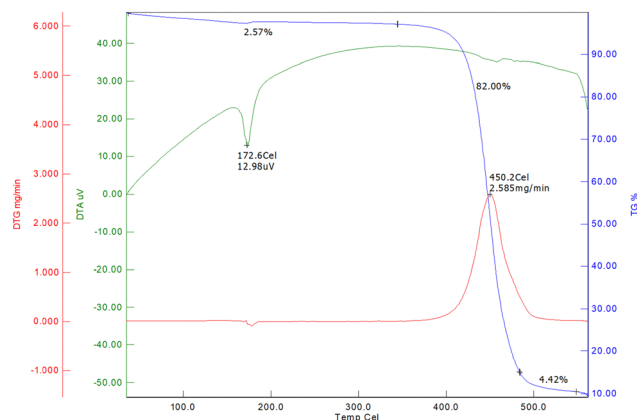

Fig. 5 TGA curve for dimer **CB6AZ**.

software to conduct theoretical calculations essential for understanding molecular properties, such as optimized structures and vibrational frequencies.[39–44] The process began with optimizing the energy of different conformations to determine the geometrical structure with the lowest energy. Subsequently, the optimized structure served as the basis for calculating frequencies and thermodynamic properties. Our depiction of molecular structures adheres to a specific colour scheme: carbon atoms are depicted in grey, nitrogen in blue, oxygen in red, and hydrogen in white. The intricate three-dimensional arrangement of the molecules under investigation arises from the precise spatial arrangement of atoms, interconnected through Sigma and pi bonds. Fig. 6 presents the optimized molecular structures of the dimers from both series, offering significant insights into their structural properties as derived from our computational analysis.

Table 2 presents the stabilization energy or energy minima values, expressed in Hartree, for each dimer. As depicted in Fig. 7, energy minima progressively decrease with an increase
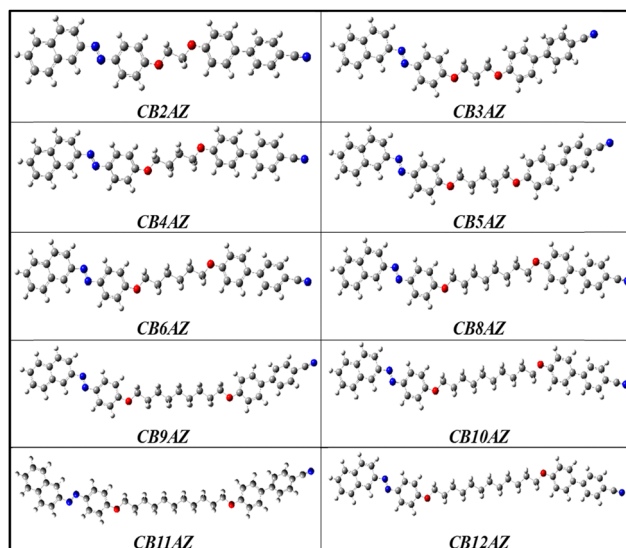

Fig. 6 Optimized molecular structures of series **CBnAZ**.

This journal is © The Royal Society of Chemistry 2025

J. Mater. Chem. C, 2025, **13**, 10700–10713 | **10705**

Table 2 DFT-computed quantum mechanical descriptors of series **CB*n*AZ**

Dimer	Energy minima (Hartree)	HOMO	LUMO	I (eV)	A (eV)	ΔE (eV)	η	$\delta = 1/\eta$	χ	ω
CB2AZ	−1509.842	−0.209	−0.083	5.678	2.251	3.427	1.714	0.584	3.965	4.586
CB3AZ	−1549.160	−0.208	−0.082	5.648	2.225	3.423	1.712	0.584	3.936	4.526
CB4AZ	−1588.478	−0.206	−0.081	5.615	2.193	3.422	1.711	0.584	3.904	4.454
CB5AZ	−1627.795	−0.206	−0.080	5.597	2.177	3.420	1.710	0.585	3.887	4.418
CB6AZ	−1667.111	−0.205	−0.079	5.578	2.159	3.419	1.709	0.585	3.869	4.378
CB8AZ	−1745.745	−0.204	−0.079	5.556	2.139	3.417	1.708	0.585	3.847	4.332
CB9AZ	−1785.061	−0.203	−0.077	5.548	2.119	3.429	1.714	0.583	3.833	4.285
CB10AZ	−1824.378	−0.204	−0.078	5.541	2.125	3.416	1.708	0.585	3.833	4.301
CB11AZ	−1863.695	−0.203	−0.077	5.536	2.104	3.432	1.716	0.582	3.820	4.252
CB12AZ	−1903.011	−0.203	−0.078	5.532	2.116	3.416	1.708	0.586	3.824	4.280

Ionization potential (I); electron affinity (A); energy gap (ΔE); global hardness (η); global softness (δ); chemical reactivity (χ); electrophilicity index (ω)

in the no. of carbon atoms in the flexible spacer chain of the dimers. The electronic characteristics, specifically the energies of the highest occupied molecular orbital (HOMO) and the lowest unoccupied molecular orbital (LUMO), were determined for the optimized structures. An investigation of the frontier molecular orbitals (FMOs) was performed to predict the stability and chemical reactivity of the dimers. To assess the potential for electron transfer in the compounds, the energy gap between the HOMO and LUMO was computed. In the **CB*n*AZ** series, the HOMO and LUMO are mainly derived from the π-orbitals of the naphthyl ring, with a small contribution from the azo linkage (–N=N–). The LUMO, in particular, corresponds to the anti-bonding orbital of the biphenyl ring that has a cyano group attached (Fig. 8). The spatial distribution of electron densities within the molecular orbitals (MOs) is not significantly influenced by the length of the flexible spacer. As shown in Table 2, extending the length of the spacer does not notably alter the energy gap. The high charge density around the cores of the dimers, as illustrated in Fig. 8, accounts for the consistency observed in the energy gap. Notably, the dimers studied displayed almost identical values for parameters such as chemical hardness (η) and softness (δ), regardless of the length of the flexible spacer chains.

In the series of dimers, each molecule has a dipole moment ranging from approximately 4.6 to 5.2 Debye (Table 3). Typically, molecular interactions significantly impact dipole moments. Notably, odd-membered dimers have lower dipole moments than even-membered dimers. Table 3 also shows the polarizability values for both series **CB*n*AZ**, revealing a significant correlation between polarizability and the length of the flexible spacer. As the chain length increases, polarizability also increases proportionally. The odd-membered dimers have a greater molecular breadth due to their bent shape, resulting in lower aspect ratio values. Dimers with tetramethylene and hexamethylene spacers exhibit a higher mesophase range compared to other dimers. Furthermore, odd-membered dimers do not display liquid crystal properties during the heating cycle.

The molecular electrostatic potential (MEP) surface was created to visualize the distribution of electron density, which helps predict the sites for electrophilic and nucleophilic attacks. Additionally, mesophase formation in these compounds is impacted by molecular packing arrangements, which are likely influenced by charge distribution. In this study, the charge distribution was analyzed with the B3LYP/6-31G basis set. Fig. 9 illustrates the MEP surface, which is crucial for understanding these interactions. Electrophiles are attracted to regions with higher negative charge (red areas), whereas nucleophiles are drawn to regions with less negative charge (blue areas). The charge separation within the dimers induces end-to-end interactions, resulting in the formation of a nematic mesophase with restricted lateral ordering. Red regions are primarily concentrated around the cyano groups and nitrogen atoms of the azo groups, whereas blue regions are generally observed along the carbon chain of the flexible spacer. The distinct odd–even effects seen in the transitional properties of the dimers are driven by their molecular configuration, which depends on the number of atoms linking the mesogenic units. Dimers with an even number of atoms usually adopt a linear shape, while those with an odd number of atoms generally have a bent shape. The structural difference influences their compatibility within the molecular arrangement of the nematic phase, leading to variations in transitional behaviours, such as shifts in melting points and nematic–isotropic transition temperatures, as shown in Fig. 10.

The calculated vibrational frequencies of the dimers were compared with the experimental values obtained from the FT-IR spectra. The theoretical frequencies showed good agreement with the experimental values, confirming the accuracy of the

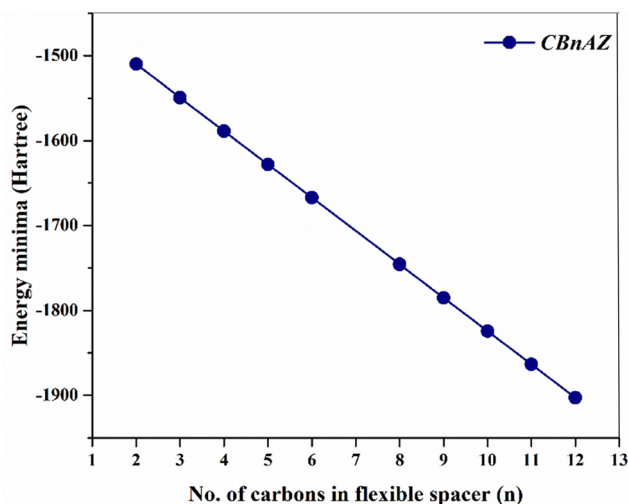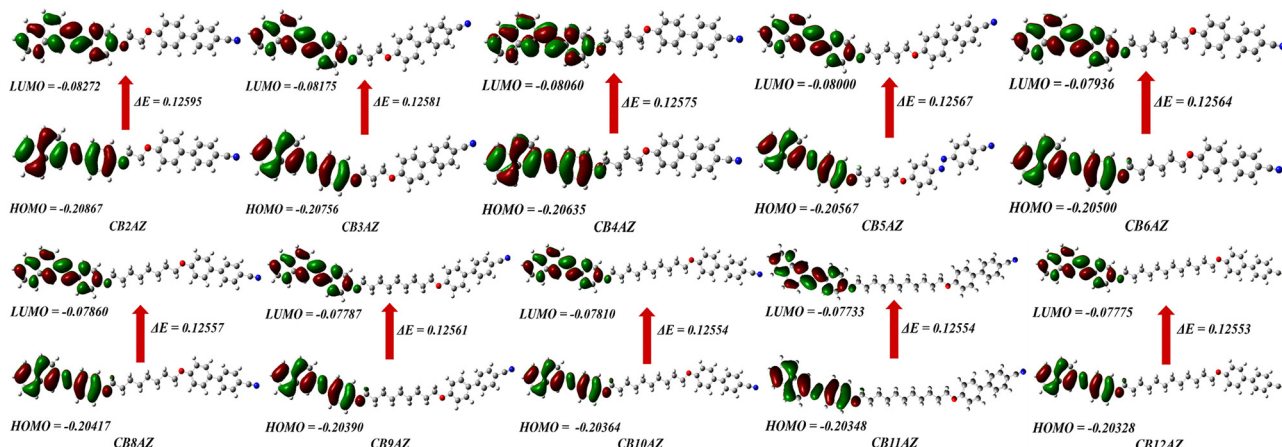**Fig. 7** A plot depicting the variation in energy minima as the length of the flexible spacer chain increases in the **CB*n*AZ** dimer series.

10706 | *J. Mater. Chem. C*, 2025, **13**, 10700–10713

This journal is © The Royal Society of Chemistry 2025

LUMO = -0.08272   ΔE = 0.12595   LUMO = -0.08175   ΔE = 0.12581   LUMO = -0.08060   ΔE = 0.12575   LUMO = -0.08000   ΔE = 0.12567   LUMO = -0.07936   ΔE = 0.12564

HOMO = -0.20867   HOMO = -0.20756   HOMO = -0.20635   HOMO = -0.20567   HOMO = -0.20500

CB2AZ   **CB3AZ**   **CB4AZ**   **CB5AZ**   **CB6AZ**

LUMO = -0.07860   ΔE = 0.12557   LUMO = -0.07787   ΔE = 0.12561   LUMO = -0.07810   ΔE = 0.12554   LUMO = -0.07733   ΔE = 0.12554   LUMO = -0.07775   ΔE = 0.12553

HOMO = -0.20417   HOMO = -0.20390   HOMO = -0.20364   HOMO = -0.20348   HOMO = -0.20328

CB8AZ   **CB9AZ**   **CB10AZ**   **CB11AZ**   **CB12AZ**

Fig. 8 Frontier molecular orbitals (FMOs) of the **CBnAZ** dimer series (HOMO, LUMO, and ΔE values in a.u.).

Table 3 Optical properties and dimensional parameters of the dimers

Dimer	Dipole moment μ (Debye)	Polarizability α (a.u.)	Length (L) Å	Width (D) Å	Aspect ratio (L/D)	Mesophase range (ΔT) °C
CB2AZ	5.202	439.038	27.798	5.569	4.991	18.06
CB3AZ	4.987	449.331	28.340	7.779	3.643	—
CB4AZ	5.098	461.590	30.295	5.569	5.439	40.68
CB5AZ	4.922	472.091	30.882	7.776	3.971	—
CB6AZ	5.045	484.010	32.803	5.568	5.891	47.56
CB8AZ	5.011	506.503	35.323	5.567	6.345	40.77
CB9AZ	4.867	517.544	36.008	7.689	4.683	26.52
CB10AZ	4.991	529.138	37.847	5.565	6.800	37.14
CB11AZ	4.615	540.735	38.391	7.625	5.034	25.71
CB12AZ	4.978	551.819	40.376	5.563	7.257	34.92

DFT calculations. The obtained geometries were further confirmed by the vibrational frequency analysis, which yielded no imaginary frequency. Fig. 11 presents a comparison between the experimental and theoretical vibrational frequencies for the **CB6AZ** dimer, calculated using the B3LYP-6-31G level of theory.

The vibrational modes of the phenyl and naphthalene rings include C–H stretching vibrations in the range of 2800–3000 cm^{-1}, in-plane and out-of-plane C–H bending vibrations between 700–850 cm^{-1}, and –C≡C– stretching vibrations between 1500–1570 cm^{-1}, with a strong agreement observed between the theoretical and experimental values. C–C stretching vibrations are observed between 1450–1300 cm^{-1}, while in-plane C–C bending vibrations occur at around 1010–1030 cm^{-1}. Vibrations at 1600 cm^{-1} indicate a –N═N– double bond. The cyano group (nitrile) exhibits C–N stretching vibrations at 2220 cm^{-1}. Ether groups display C–O stretching vibrations (1260–1200 cm^{-1}) and O–C–O bending vibrations (720–640 cm^{-1}) in line with theoretical calculations.

3.6. Photoswitching behaviour

The absorption spectra for *trans–cis* photoisomerization and *cis–trans* thermal back relaxation were recorded in solution. These experiments were conducted in a dark room at room
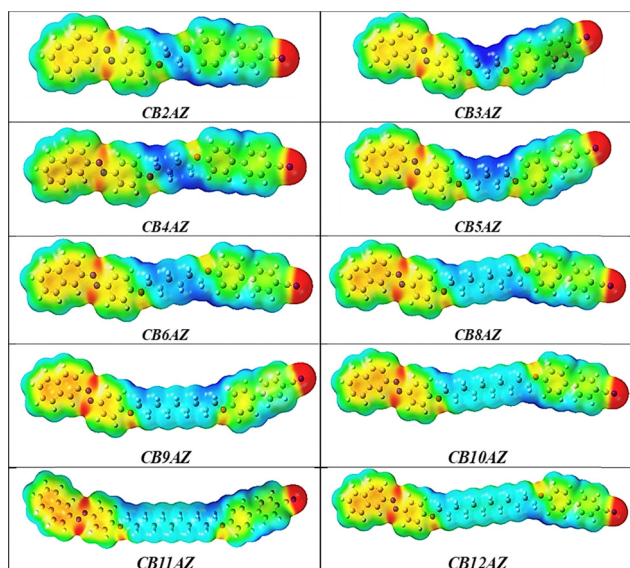

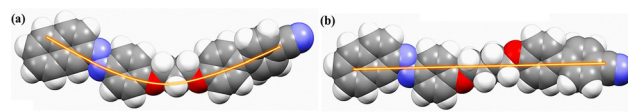**Fig. 9** MEP contours of the dimers of **CBnAZ**.

Fig. 10 Space-filling models of (a) **CB3AZ** (odd-membered dimer) and (b) **CB4AZ** (even-membered dimer), illustrating the spacer in the all-trans configuration.
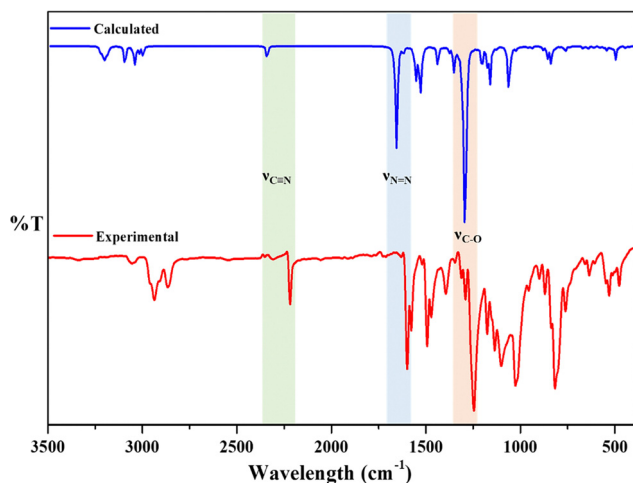
Fig. 11 Comparison of the experimental vibrational frequencies with calculated frequencies at the B3LYP-6-31G level of theory (gas phase) for the **CB6AZ** dimers.

temperature (27 ± 1 °C) with the compounds dissolved in chloroform at a fixed concentration of approximately 1.0×10^{-5} mol L^{-1}. The prepared samples were placed in a quartz cuvette (1 cm optical length) and positioned in the sample holder. The samples were then exposed to UV light with an intensity of around 1 mW cm^{-2}, provided by an OMNICURE series 2000 UV light source, which was fitted with a heat filter to eliminate heat radiation and a 365 nm UV filter. The absorption spectra were first measured under UV irradiation at various exposure times, followed by spectra of compounds undergoing thermal back relaxation at different time intervals.

The photo-switching behaviour of the azobenzene molecules was studied by examining the influence of different chain lengths ($n = 2$–12) for the dimers of series **CB*n*AZ**. Prior to UV illumination, the absorption spectra of all dimers showed a significant peak around 358–361 nm, corresponding to the symmetry-allowed π–π* transition of the azo moiety, along with a weaker peak around 450 nm due to the symmetry-forbidden n–π* transition. Upon UV irradiation, the compounds underwent *trans–cis* photoisomerization, with a gradual decrease in the absorbance maximum near 365 nm, indicative of the *trans–cis* conversion, and a slight increase in the peak at approximately 450 nm. As shown in Table 4 and Fig. 12, all compounds

Table 4 Showing the *E–Z* and *Z–E* relaxation along with conversion efficiency

Dimer	Time for *E–Z* in seconds (∼)	Time for *Z–E* in minutes	CE (%)
CB2AZ	49	600	88.70
CB3AZ	50	660	86.55
CB4AZ	50	720	95.19
CB5AZ	49	660	96.09
CB6AZ	48	600	94.23
CB8AZ	49	660	94.79
CB9AZ	47	600	94.77
CB10AZ	49	720	95.01
CB11AZ	48	600	96.13
CB12AZ	50	660	95.85

exhibited similar photo-saturation times of approximately 45–50 seconds, suggesting that this behaviour depends solely on the UV intensity and is not influenced by the terminal groups or the length of the flexible spacer chain. The changes in the absorption peaks due to UV exposure are depicted in Fig. 12a–j, with the peak absorbance values plotted over time in Fig. 12k.

One can observe from Table 4 that all the compounds show a similar conversion efficiency rate of 88–95% indicating the high sensitivity of the molecules under UV irradiation. Out of all of them, **CB11AZ** shows the highest conversion efficiency of 96% and **CB2AZ** has the lowest conversion efficiency of 88%.

Within 50 seconds of illumination, entire *trans* molecules converted to *cis* molecules indicating high conversion efficiency in such systems. The photo-conversion efficiency, as shown in eqn (1), can be used to determine the extent of photoisomerization.

$$\text{PCE} = \frac{A(t_0) - A(t_\infty)}{A(t_0)} \times 100 \tag{1}$$

Here $A(t_0)$ is the initial absorbance (before UV exposure) and $A(t_\infty)$ is the final absorbance (after UV exposure).

When the photo-induced saturation state is achieved, the molecular conformations, depending on their structure, remain stable for a considerable period. However, the *cis*-to-*trans* conversion can be triggered either by irradiating with white light at 450 nm or by keeping the system in the dark, which is referred to as thermal back relaxation. Since the ability to recover conformations without external irradiation is vital for optical storage applications, thermal back relaxation is preferred. To assess the back-relaxation time without the influence of external light, absorbance spectra were recorded for solutions in the dark. Fig. 13a–j illustrates the absorbance changes occurring during the thermal back-relaxation process, while Fig. 13k shows the peak absorbance values plotted over time. The variation in thermal back-relaxation time can be attributed to the influence of the terminal groups and the spacer length in the dimer structures. One can see from the figure and Table 4 that thermal back relaxation for all the compounds ranged between 10–12 hours, where **CB2AZ** will be the lowest and **CB10AZ** will be the highest thermal back relaxation times.

3.6.1. Kinetic studies. The kinetics of thermal isomerization provide valuable insights into the effects of both time and temperature on the process. The first-order plot of $-k_{C-t}t$ *versus* the thermal relaxation time for the studied compounds at room temperature can be generated by determining $-k_{C-t}t$ using eqn (2)

$$\ln \frac{A_\infty - A_t}{A_\infty - A_0} = -k_{C-t}t \tag{2}$$

where A_0, A_t and A_∞ are the peak absorbance values at time zero, time t and time infinity, respectively. Fig. 14 shows the first-order to second-order plot for the compound **CB*n*AZ** series. The system demonstrated first-order kinetics for up to 400 minutes, as evident from the linear plot. However, deviations from first-order kinetics were observed in dimers with extended thermal back relaxation times, likely influenced by minor temperature fluctuations during the study.

10708 | *J. Mater. Chem. C*, 2025, **13**, 10700–10713

This journal is © The Royal Society of Chemistry 2025

Fig. 12 Absorption spectra as a function of UV exposure time for: (a) **CB2AZ**, (b) **CB3AZ**, (c) **CB4AZ**, (d) **CB5AZ**, (e) **CB6AZ**, (f) **CB8AZ**, (g) **CB9AZ**, (h) **CB10AZ**, (i) **CB11AZ**, and (j) **CB12AZ**. (k) Variation of peak absorbance extracted from (a) to (j) plotted against UV irradiation time. The UV light intensity is maintained at 1 mW cm^{-2}, and a heat filter is placed between the solution and the UV light source to eliminate any thermal effects caused by the light.

3.6.2. The reason behind the phenomenon. The study of liquid crystal materials containing azobenzene moieties with varying chain lengths at the core is particularly fascinating due to the competing effects that arise under exposure to specific wavelengths of light. In their initial state, these molecules exhibit a rod-like shape. However, upon illumination with UV light at a wavelength of 365 nm, their structure undergoes a transformation, adopting a distorted bent configuration. In a guest–host system used in practical devices, these molecules align as rod-like entities alongside the host liquid crystals. When exposed to UV light at 365 nm, their flexible core structure prompts a shift to a distorted bent orientation. This change also influences the host liquid crystals, causing them to remain in the bent configuration for extended periods due to increased thermal back relaxation times. In view of this we tried here to explain the observed phenomena using three distinct cases (see Fig. 15 for the cartoon diagram). Here we chose three cases such as $n = 2$, $n = 6$ and $n = 12$ to understand the influence of the spacer length on the guest–host systems.

Case 1: n = 2. When spacer length $n = 2$ in the guest–host system, both liquid crystal host molecules and the guest unsymmetrical dimers are happy to be in the rod shape. As soon as UV light of wavelength ∼365 nm is shined on them, host liquid crystal molecules change from an ordered nematic

phase to a disordered isotropic phase whereas dimers will change their configuration. Near the –N═N– linkage they slightly bend and this bending will dictate the remaining structure to follow. Due to this, some kind of rope structure is formed (as shown in Fig. 16), which prevents the host liquid crystalline molecules from relaxing back quickly to their original configuration.

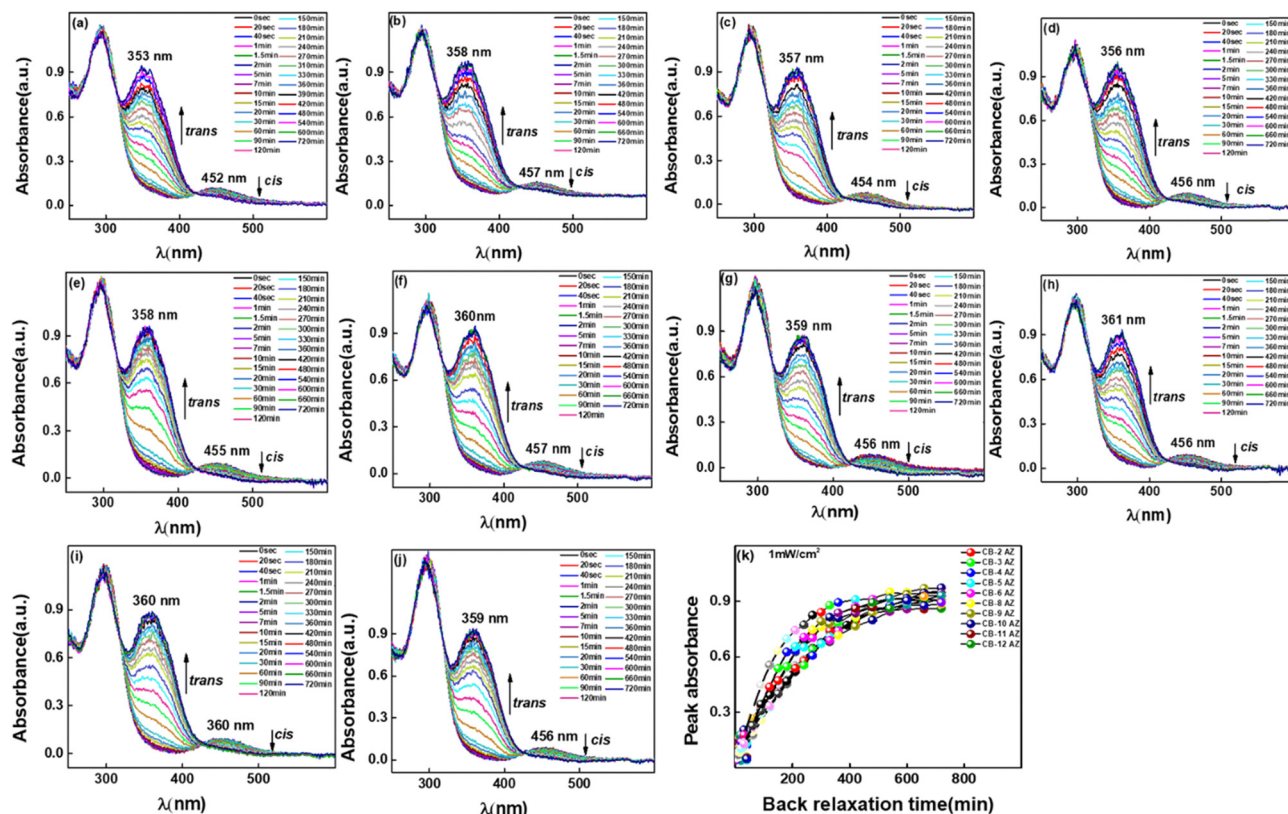*Case 2: n = 6.* When spacer length $n = 6$ in the guest–host system, both liquid crystal host molecules and the guest unsymmetrical dimers are happy to be in the rod shape before shining the UV light on them. As soon as UV light of wavelength ∼365 nm is shined on them, host liquid crystal molecules change again from an ordered nematic phase to a disordered isotropic phase whereas unsymmetrical dimers will change their configuration. Near to the –N═N– linkage they bend substantially due to the longer spacer length and this bending will dictate the remaining structure to follow. Due to this some kind of coiled structure is formed (as shown in Fig. 17), which prevents the host liquid crystalline molecules from relaxing back quickly to their original configuration.

Case 3: n = 12. When spacer length $n = 12$ in the guest–host system, both liquid crystal host molecules and the guest unsymmetrical dimers are happy to be in the rod shape before

This journal is © The Royal Society of Chemistry 2025

J. Mater. Chem. C, 2025, **13**, 10700–10713 | **10709**

Fig. 13 Thermal back relaxation studies of the **CB*n*AZ** series (*n* = 2–12) following UV irradiation are shown in ''a'' to ''j''. The plot of peak absorbance *versus* time, representing thermal back relaxation behaviour derived from ''a'' to ''j,'' is illustrated in ''k.'' One can see that within 500 minutes most of the *cis* molecules are converted back to *trans* molecules.
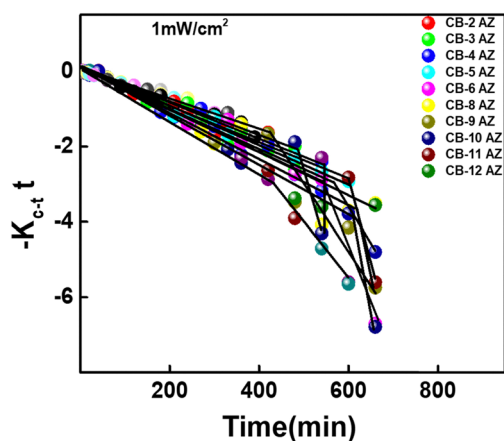

Fig. 14 Plots depicting first-order and second-order kinetics for the thermal *cis–trans* isomerization of the studied dimers.

shining the UV light on them. As soon as UV light of wavelength ~365 nm is shined on them, host liquid crystal molecules change again from an ordered nematic phase to a disordered isotropic phase, whereas unsymmetrical dimers will change their configuration. Near to the –N═N– linkage they bend drastically due to the longer spacer length and this bending will dictate the remaining structure to follow. Due to this a
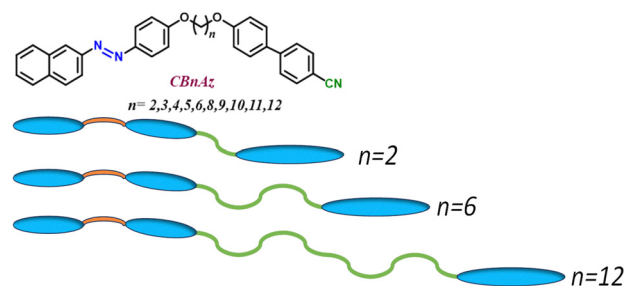

Fig. 15 Cartoon diagram showing the distribution of spacer length along with the chemical structure.
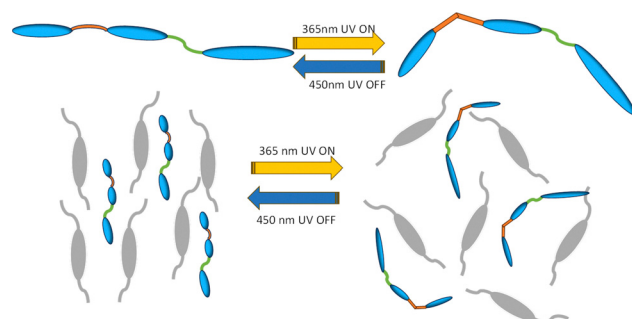

Fig. 16 Picture depicting the situation where spacer length is fixed at *n* = 2.

10710 | *J. Mater. Chem. C*, 2025, **13**, 10700–10713

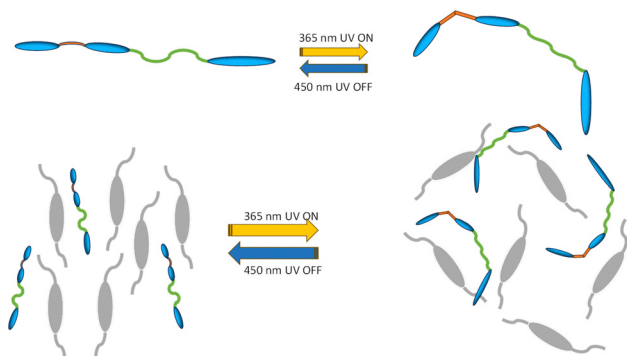This journal is © The Royal Society of Chemistry 2025

Fig. 17 Picture depicting the situation where spacer length is fixed at $n = 6$.

completely coiled structure is formed (as shown in Fig. 18), which prevents the host liquid crystalline molecules from relaxing back quickly to their original configuration.

In all the three cases, always unsymmetrical dimers create a difficult situation for the host molecules to relax back to the original configuration. Since this bending is happening at one end and the spacer is changing length at the other end, the overall chemical structure remains more or less the same except for the flexibility in the middle of the structure. Perhaps, in the future one can add spacer length at the end of the benzene ring to lead to different back relaxation times with respect to the change in the spacer length. A study on this is in progress and will be reported elsewhere.

3.6.3. Device fabrication. The optical storage device is fabricated using an unsymmetrical dimer **CB11AZ** ($n = 11$ which showed the highest conversion efficiency) as the guest molecule and E7, room temperature liquid crystal as the host molecules. Here we mixed 5% of the guest unsymmetrical dimers in 95% of the host E7 molecules. A previously prepared ITO-coated rubbed polyimide cell is filled with the guest–host mixture using capillary action. After filling, a suitable mask is kept on top of the liquid crystal cell and UV light of wavelength 5 mW cm^{-2} is shined for 2 minutes. After that, the mask was removed and the device was seen through crossed polarizers.
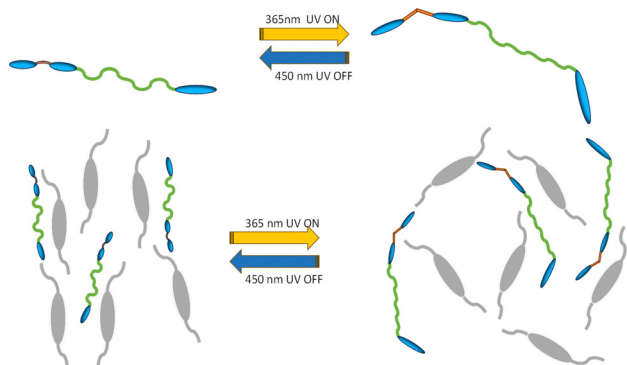

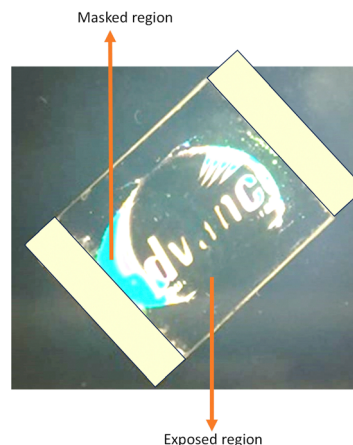**Fig. 18** Picture depicting the situation where spacer length is fixed at $n = 12$.

Fig. 19 Optical storage device fabricated using **CB11AZ**, where dimers were used as the guest molecule and the liquid crystal E7 was used as the host molecule. One can see from the device that the exposed region corresponds to the UV illumination (dark state) and the masked region is corresponding to that UV-protected area through the mask (dark state).

One can see from Fig. 19 that, wherever the mask is protected, liquid crystal molecules remain in the ordered nematic phase (bright state) and wherever UV is exposed to them, they turn to the isotropic phase (dark state). One can clearly see the excellent contrast between the dark and the white states from the unsymmetrical dimers incorporated in the system.

The current study depicts that, proper tuning of the spacers inside the chemical structure can enhance the device performance drastically and also a strong structure–property relationship is the key to success in the area of optical storage devices.

4. Conclusion

The series **CB*n*AZ** demonstrated mesogenic behaviour, characterized by enantiotropic nematic phases and, in certain cases, the presence of monotropic smectic C phases. The study revealed that the length of the flexible spacer significantly influences the thermotropic properties, with longer spacers leading to lower transition temperatures due to increased flexibility and reduced intermolecular forces. The odd–even effect further impacted the mesophase behaviour, where odd-membered dimers, particularly those with $n = 3$ and $n = 5$, exhibited lower clearing temperatures and monotropic nematic phase. Interestingly, in the case of $n = 11$, both nematic and smectic phases were observed, suggesting a diminishing odd–even effect with longer chains. As the chain length increased from $n = 8$ to $n = 12$, the emergence of smectic phases became more prominent, indicative of layered structures with long-range positional order, whereas shorter chains predominantly exhibited nematic phases. Additionally, photo-switching studies *via* UV-visible spectroscopy showed consistent conversion efficiencies of 88–95% across all dimers, highlighting their high sensitivity to UV irradiation along with a thermal back relaxation time of ∼500 minutes (irrespective of the spacer

This journal is © The Royal Society of Chemistry 2025

J. Mater. Chem. C, 2025, **13**, 10700–10713 | **10711**

length). These findings underscore the critical role of molecular architecture in determining the mesogenic and photochromic properties of these liquid crystal dimers. An optical storage device was also fabricated showing excellent dark and bright contrast depicting the feasibility of the materials for further investigations.

Data availability

The data supporting this article have been included as part of the ESI.†

Conflicts of interest

The authors declare that they have no known competing financial interests or personal relationships or conflicts of interest that could have appeared to influence the work reported in this paper.

Acknowledgements

References

1 G. W. Gray, *Mol. Cryst.*, 1969, **7**, 127–151.
2 R. J. Mandle and J. W. Goodby, *RSC Adv.*, 2016, **6**, 34885–34893.
3 D. Dunmur, *Crystals*, 2022, **12**, 309.
4 I. Dozov, *Europhys. Lett.*, 2001, **56**, 247.
5 R. Memmer, *Liq. Cryst.*, 2002, **29**, 483–496.
6 V. P. Panov, M. Nagaraj, J. K. Vij, Y. P. Panarin, A. Kohlmeier, M. G. Tamba, R. A. Lewis and G. H. Mehl, *Phys. Rev. Lett.*, 2010, **105**, 167801.
7 Y. Cao, J. Feng, A. Nallapaneni, Y. Arakawa, K. Zhao, H. Zhang, G. H. Mehl, C. Zhu and F. Liu, *J. Mater. Chem. C*, 2021, **9**, 10020–10028.
8 V. Borshch, Y.-K. Kim, J. Xiang, M. Gao, A. Jákli, V. P. Panov, J. K. Vij, C. T. Imrie, M. G. Tamba, G. H. Mehl and O. D. Lavrentovich, *Nat. Commun.*, 2013, **4**, 2635.
9 D. Chen, J. H. Porada, J. B. Hooper, A. Klittnick, Y. Shen, M. R. Tuchband, E. Korblova, D. Bedrov, D. M. Walba, M. A. Glaser, J. E. Maclennan and N. A. Clark, *Proc. Natl. Acad. Sci. U. S. A.*, 2013, **110**, 15931–15936.
10 P. K. Challa, V. Borshch, O. Parri, C. T. Imrie, S. N. Sprunt, J. T. Gleeson, O. D. Lavrentovich and A. Jákli, *Phys. Rev. E:Stat., Nonlinear, Soft Matter Phys.*, 2014, **89**, 60501.
11 K. Merkel, B. Loska, Y. Arakawa, G. H. Mehl, J. Karcz and A. Kocot, *Int. J. Mol. Sci.*, 2022, **23**, 11018.

12 J. Zhou, W. Tang, Y. Arakawa, H. Tsuji and S. Aya, *Phys. Chem. Chem. Phys.*, 2020, **22**, 9593–9599.
13 M. P. Kumar, P. Kula and S. Dhara, *Phys. Rev. Mater.*, 2020, **4**, 115601.
14 N. Sebastián, D. O. López, B. Robles-Hernández, M. R. de la Fuente, J. Salud, M. A. Pérez-Jubindo, D. A. Dunmur, G. R. Luckhurst and D. J. B. Jackson, *Phys. Chem. Chem. Phys.*, 2014, **16**, 21391–21406.
15 T. Ivšić, M. Vinković, U. Baumeister, A. Mikleušević and A. Lesac, *RSC Adv.*, 2016, **6**, 5000–5007.
16 C. T. Archbold, E. J. Davis, R. J. Mandle, S. J. Cowling and J. W. Goodby, *Soft Matter*, 2015, **11**, 7547–7557.
17 K. Adlem, M. Čopič, G. R. Luckhurst, A. Mertelj, O. Parri, R. M. Richardson, B. D. Snow, B. A. Timimi, R. P. Tuffin and D. Wilkes, *Phys. Rev. E:Stat., Nonlinear, Soft Matter Phys.*, 2013, **88**, 22503.
18 D. A. Paterson, M. Gao, Y.-K. Kim, A. Jamali, K. L. Finley, B. Robles-Hernández, S. Diez-Berart, J. Salud, M. R. de la Fuente, B. A. Timimi, H. Zimmermann, C. Greco, A. Ferrarini, J. M. D. Storey, D. O. López, O. D. Lavrentovich, G. R. Luckhurst and C. T. Imrie, *Soft Matter*, 2016, **12**, 6827–6840.
19 Z. Lu, P. A. Henderson, B. J. A. Paterson and C. T. Imrie, *Liq. Cryst.*, 2014, **41**, 471–483.
20 R. J. Mandle, E. J. Davis, S. A. Lobato, C.-C. A. Vol, S. J. Cowling and J. W. Goodby, *Phys. Chem. Chem. Phys.*, 2014, **16**, 6907–6915.
21 R. J. Mandle, C. C. A. Voll, D. J. Lewis and J. W. Goodby, *Liq. Cryst.*, 2016, **43**, 13–21.
22 A. A. Dawood, M. C. Grossel, G. R. Luckhurst, R. M. Richardson, B. A. Timimi, N. J. Wells and Y. Z. Yousif, *Liq. Cryst.*, 2017, **44**, 106–126.
23 Y. Arakawa, K. Komatsu, T. Shiba and H. Tsuji, *Mater. Adv.*, 2021, **2**, 1760–1773.
24 D. Wang, J. Liu, W. Zhao, Y. Zeng, J. Huang, J. Fang and D. Chen, *Chem. - Eur. J.*, 2022, **28**(70), e202202146.
25 Y. Arakawa, Y. Ishida and H. Tsuji, *Chem. - Eur. J.*, 2020, **26**, 3787.
26 Y. Arakawa, K. Komatsu, Y. Ishida and H. Tsuji, *Liq. Cryst.*, 2021, **48**, 641–652.
27 D. A. Paterson, R. Walker, J. M. D. Storey and C. T. Imrie, *Liq. Cryst.*, 2023, **50**, 725–736.
28 D. A. Paterson, R. Walker, J. P. Abberley, J. Forestier, W. T. A. Harrison, J. M. D. Storey, D. Pociecha, E. Gorecka and C. T. Imrie, *Liq. Cryst.*, 2017, **44**, 2060–2078.
29 D. S. Kumari, A. Shetty, B. S. Ranjitha, M. Vandana, G. Shanker, M. Alaasar and G. Hegde, *Heliyon*, 2024, **10**, e37455.
30 M. L. Rahman, T. Xin Ting, M. S. Sarjadi, S. E. Arshad, S. Soloi, Z. Jamain, M. H. Abd Majid and G. Hedge, *J. Macromol. Sci., Part A:Pure Appl. Chem.*, 2024, **61**, 40–52.
31 B. S. Ranjitha, D. Sandhya Kumari, A. Shetty, G. Shanker, M. Alaasar, R. Pashameah and G. Hegde, *J. Mol. Liq.*, 2023, **383**, 121985.
32 J. M. Shivanna, M. Alaasar and G. Hegde, *J. Mol. Liq.*, 2021, **341**, 117341.

33 B. N. Sunil, M. Monika, G. Shanker, G. Hegde and V. Prasad, *Front. Phys.*, 2021, **9**, 728632.

34 S. M. Gan, A. R. Yuvaraj, M. R. Lutfor, M. Y. Mashitah and H. Gurumurthy, *RSC Adv.*, 2015, **5**, 6279–6285.

35 G. Hegde, G. Shanker, S. M. Gan, A. R. Yuvaraj, S. Mahmood and U. K. Mandal, *Liq. Cryst.*, 2016, **43**, 1578–1588.

36 M. Rabari and A. K. Prajapati, *J. Mol. Struct.*, 2024, **1307**, 137971.

37 M. Rabari and A. K. Prajapati, *J. Mol. Struct.*, 2024, **1308**, 138101.

38 M. Rabari, R. S. Kumar CH and A. K. Prajapati, *J. Mol. Struct.*, 2023, **1293**, 136252.

39 J. P. Cornard, L. Dangleterre and C. Lapouge, *J. Phys. Chem. A*, 2005, **109**, 10044–10051.

40 S. Sundaram, V. N. Vijayakumar and V. Balasubramanian, *Comput. Theor. Chem.*, 2022, **1217**, 113920.

41 M. J. Sani, *Comput. Theor. Chem.*, 2023, **1223**, 114100.

42 R. Kumar Yadav, B. Yadav and R. A. Yadav, *Comput. Theor. Chem.*, 2023, **1228**, 114264.

43 L. Piela, *Ideas of Quantum Chemistry*, Elsevier, 2020, 3rd edn, pp. 191–252.

44 H. Henschel, A. T. Andersson, W. Jespers, M. Mehdi Ghahremanpour and D. van der Spoel, *J. Chem. Theory Comput.*, 2020, **16**, 3307–3315.

This journal is © The Royal Society of Chemistry 2025

J. Mater. Chem. C, 2025, **13**, 10700–10713 | **10713**